Exactly soluble model of continuum-continuum transitions in strong laser beams

Z. Bialynicka-Birula
Institute of Physics, Polish Academy of Sciences, 02-668 Warsaw, Poland
(Received 8 April 1982)

A model of continuum-continuum transitions induced by very intense laser beams is solved. The energy distribution of the photoelectrons is found and it exhibits the broadening and the splitting induced by the laser field. Similar effects are known for bound-bound transitions, but our model made it possible to study them systematically in the continuum.

I. INTRODUCTION

There is renewed interest in the dynamics of the continuum-continuum transitions in atoms induced by laser light, owing to the recent experimental evidence of such a process.[1] Following Lambropoulos,[2] I will use the term continuum-continuum transition (cc transition) to describe an optical transition from a lower state in the continuum to a higher state in the continuum, when this transition is coherent with the whole process of excitation from the initial bound state. When the laser field is not too strong, the cc transition can be adequately described with the help of the perturbation method.[3] For very high intensities the perturbation method fails and the problem is very difficult to solve. However, it becomes somewhat simpler when, owing to the existence of autoionizing states,[4] there are regions in the continuum with an exceptionally high density of states and the cc transitions occur between the states lying in those regions. Such processes may be viewed as something intermediate between the cc transitions in a smooth continuum and the transitions between bound states. Therefore we can expect that an intense laser light will cause in those processes effects similar to the saturation phenomena in bound-bound transitions, but that they will be modified by the presence of the continuum. Certain theoretical aspects of these problems have already been studied by Rzążewski and Eberly[5] and by Lambropoulos and Zoller.[6]

The purpose of this work was to evaluate the effects of a strong laser field on the cc transitions in a a simple, exactly soluble, theoretical model. I believe that the results obtained in this way are at least qualitatively valid in a more realistic theory.

II. THE MODEL

The physical system described by the model is composed of an atom and two kinds of photons with the frequencies ω_1 and ω_2. The atom is assumed to have one discrete bound state $|g\rangle$ with the energy E_g and two families of states $|{}_1E\rangle$ and $|{}_2E\rangle$ belonging to the continuous spectrum with the energy E extending from E_0 to infinity. The states $|{}_2E\rangle$ have the same parity as the bound state $|g\rangle$, whereas the states $|{}_1E\rangle$ have the opposite parity and can be reached from the bound state by a single photon transition.

The atomic state vectors will be normalized as follows:

$$\langle g \mid g\rangle = 1 , \tag{1a}$$

$$\langle {}_iE \mid {}_jE'\rangle = \delta_{ij}\delta(E-E'), \quad i,j=1,2 . \tag{1b}$$

I assume an especially simple form of the interaction between the atom and the electromagnetic field, which leads to the solubility of the model. The interaction Hamiltonian H_I has the following form ($\hbar = 1 = c$):

$$H_I = \int_{E_0}^{\infty} dE\, D_1(E) \mid {}_1E\rangle\langle g \mid a_1 + \int_{E_0}^{\infty} dE\, D_1^*(E) \mid g\rangle\langle {}_1E \mid a_1^\dagger + \lambda \int_{E_0}^{\infty} dE' \int_{E_0}^{\infty} dE\, D_2(E') D_1^*(E) \mid {}_2E'\rangle\langle {}_1E \mid a_2 + \lambda \int_{E_0}^{\infty} dE' \int_{E_0}^{\infty} dE\, D_2^*(E) D_1(E') \mid {}_1E'\rangle\langle {}_2E \mid a_2^\dagger , \tag{2}$$

where a_1, a_2 and $a_1^\dagger$, $a_2^\dagger$ are the annihilation and the creation operators of the photons with the frequencies ω_1 and ω_2. The energy-dependent profiles $D_1(E)$ and $D_2(E)$ measure the strength of the coupling of the laser field to the states in the continuum. They will be specified at the later stage. They have the dimension of the square root of energy, whereas the coupling constant λ has the dimension

of one over energy.

The first two terms in the Hamiltonian H_I describe the transitions between the bound state $|g\rangle$ and the states in the continuum of the first kind $|{}_1E\rangle$ induced by an absorption or an emission of a photon with the frequency ω_1. The last two terms describe the transitions between the states $|{}_1E\rangle$ and $|{}_2E\rangle$ in the continuum, induced by a photon with the frequency ω_2.

In writing the interaction Hamiltonian in the form (2) I made two simplifying assumptions. The first one is an analog of the rotating-wave approximation and consists of neglecting all "antiresonant" terms of the form $|g\rangle\langle{}_1E|a_1$, $|{}_1E\rangle\langle g|a_1^\dagger$, $|{}_2E'\rangle\langle{}_1E|a_2$, and $|{}_1E'\rangle\langle{}_2E|a_2^\dagger$. This simplification can be justified only if the functions $D_1(E)$ and $D_2(E)$ are peaked around the energies E_1 and E_2 lying in the vicinity of $E_g+\omega_1$ and $E_g+\omega_1+\omega_2$, respectively. Therefore my model will not be well suited to describe the cc transitions in the smooth continuum, but it should work rather well for nearly resonant cc transitions in the presence of autoionizing states. The second simplifying assumption was made in the last two terms in the formula (2). Namely, I assumed that the atomic formfactor, which is in general a function of E and E', has the factorized form $D_1(E)D_2^*(E')$. Owing to these two approximations, the model can be explicitly solved.

The kinematics of the model can be described with the help of the energy diagram shown in Fig. 1.

My model can be viewed as a simplification of the theory developed by Lambropoulos and Zoller (see Sec. V of Ref. 6), which deals with two strong laser beams and two autoionizing resonances. The configuration interactions between the autoionizing states and the corresponding continua, together with the laser-induced interactions with the continua, are replaced in my model by a simple interaction between the two continua. The density of states in both continua and the effective coupling formfactors are described by two functions $D_1(E)$ and $D_2(E)$, which, by assumption, are peaked around the energies corresponding to the positions of the original autoionizing states.

Owing to its solubility, this model can also be considered as a modification of the soluble model of Beers and Armstrong[7] to accommodate for the possibility of cc transitions.

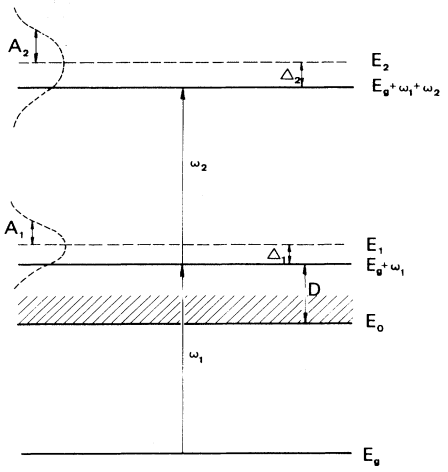

FIG. 1. Energy diagram for the continuum-continuum transition.

Since I will not introduce any additional relaxation mechanism I can solve directly the Schrödinger equation for the state vector $|\psi(t)\rangle$,

$$i\frac{d}{dt}|\psi(t)\rangle=(H_0+H_I)|\psi(t)\rangle\ , \tag{3}$$

where H_0 is the unperturbed Hamiltonian of the system,

$$H_0|g\rangle=E_g|g\rangle\ , \tag{4a}$$

$$H_0|{}_iE\rangle=E|{}_iE\rangle,\quad i=1,2 \tag{4b}$$

$$H_0|n_1,n_2\rangle=(n_1\omega_1+n_2\omega_2)|n_1,n_2\rangle\ . \tag{4c}$$

I will assume that initially (for $t=0$) the atom is in its bound state and the electromagnetic field is in a number state with large numbers of photons in both modes,

$$|\psi(t=0)\rangle=|g;n_1,n_2\rangle,\quad n_1,n_2\gg 1\ . \tag{5}$$

At a later time t the state vector has the general form:

$$|\psi(t)\rangle=U_g(t)|g;n_1,n_2\rangle+\int_{E_0}^{\infty}dE\,U_1(E,t)|{}_1E;n_1-1,n_2\rangle+\int_{E_0}^{\infty}dE\,U_2(E,t)|{}_2E;n_1-1,n_2-1\rangle\ . \tag{6}$$

My aim is to determine the probability amplitudes $U_g(t)$, $U_1(E,t)$, and $U_2(E,t)$ as functions of t and E.

The following set of equations follows from the Schrödinger equation (3) when $n_1, n_2\gg 1$:

$$i\frac{d}{dt}U_g(t)=(E_g+n_1\omega_1+n_2\omega_2)U_g(t)+\sqrt{n_1}\int_{E_0}^{\infty}dE\,D_1^*(E)U_1(E,t)\ , \tag{7a}$$

$$i\frac{d}{dt}U_1(E,t)=[E+(n_1-1)\omega_1+n_2\omega_2]U_1(E,t)+\sqrt{n_1}D_1(E)U_g(t)+\lambda\sqrt{n_2}D_1(E)\int_{E_0}^{\infty}dE'D_2^*(E')U_2(E',t)\ , \tag{7b}$$

$$i\frac{d}{dt}U_2(E,t)=[E+(n_1-1)\omega_1+(n_2-1)\omega_2]U_2(E,t)+\lambda\sqrt{n_2}D_2(E)\int_{E_0}^{\infty}dE'D_1^*(E')U_1(E',t)\ . \tag{7c}$$

They will be solved with the use of the Laplace transform. The Laplace transforms $\tilde{G}_g(p)$, $\tilde{G}_1(E,p)$, and $\tilde{G}_2(E,p)$ of the time evolution amplitudes $U_g(t)$, $U_1(E,t)$, and $U_2(E,t)$ are given by the standard formulas,

$$\tilde{G}_i(p)=\int_0^{\infty}dt\,e^{-pt}U_i(t),\quad i=g,1,2.$$

In what follows I use the variable $z=ip$ and define the functions $G_i(z)$ as $\tilde{G}_i(-iz)$. The functions $G_g(z)$, $G_1(E,z)$, and $G_2(E,z)$ satisfy the following equations, which follow from Eqs. (7) and the initial condition (5):

$$(z-E_g-n_1\omega_1-n_2\omega_2)G_g(z)-\sqrt{n_1}\int_{E_0}^{\infty}dE'D_1^*(E')G_1(E',z)=i, \tag{8a}$$

$$[z-E-(n_1-1)\omega_1-n_2\omega_2]G_1(E,z)-\sqrt{n_1}D_1(E)G_g(z)\ -\lambda\sqrt{n_2}D_1(E)\int_{E_0}^{\infty}dE'D_2^*(E')G_2(E',z)=0, \tag{8b}$$

$$[z-E-(n_1-1)\omega_1-(n_2-1)\omega_2]G_2(E,z)-\lambda\sqrt{n_2}D_2(E)\int_{E_0}^{\infty}dE'D_1^*(E')G_1(E',z)=0\ . \tag{8c}$$

The inverse Laplace transform in this case has the following form:

$$U_i(t)=\lim_{\epsilon\to 0+}\frac{1}{2\pi}\int_{-\infty}^{\infty}dx\,e^{-ixt}G_i(x+i\epsilon),\quad i=g,1,2. \tag{9}$$

The solution of Eqs. (8) has the following form:

$$G_g(z)=i\frac{1-\lambda^2 n_2\Sigma_1(z)\Sigma_2(z)}{H(z)}\ , \tag{10a}$$

$$G_1(E,z)=i\frac{\sqrt{n_1}D_1(E)}{z-E-(n_1-1)\omega_1-n_2\omega_2}\frac{1}{H(z)}\ , \tag{10b}$$

$$G_2(E,z)=i\frac{\lambda\sqrt{n_1n_2}D_2(E)}{z-E-(n_1-1)\omega_1-(n_2-1)\omega_2}\frac{\Sigma_1(z)}{H(z)}\ , \tag{10c}$$

where

$$H(z)=(z-E_g-n_1\omega_1-n_2\omega_2)[1-\lambda^2 n_2\Sigma_1(z)\Sigma_2(z)]-n_1\Sigma_1(z)\ , \tag{11}$$

and the two analytic functions $\Sigma_1(z)$ and $\Sigma_2(z)$ are defined by the following integrals:

$$\Sigma_1(z)=\int_{E_0}^{\infty}dE\frac{|D_1(E)|^2}{z-E-(n_1-1)\omega_1-n_2\omega_2}\ , \tag{12a}$$

$$\Sigma_2(z)=\int_{E_0}^{\infty}dE\frac{|D_2(E)|^2}{z-E-(n_1-1)\omega_1-(n_2-1)\omega_2}\ . \tag{12b}$$

The set of Eqs. (10) and (11) gives an analytic solution of our model for arbitrary functions $D_1(E)$ and $D_2(E)$. Notice that those functions enter not only as proportionality factors in the expressions for $G_1(E,z)$ and $G_2(E,z)$, but also through the functions $\Sigma_1(z)$ and $\Sigma_2(z)$. The Laplace transforms $G_g(z)$, $G_1(E,z)$, and $G_2(E,z)$ through Eq. (9), describe the time evolution of the system.

For those model profiles $|D_1(E)|^2$ and $|D_2(E)|^2$ which will be considered later, the functions $G_g(z)$, and $G_2(E,z)$ have two branch points at

$$E_0+(n_1-1)\omega_1+n_2\omega_2$$

and

$$E_0+(n_1-1)\omega_1+(n_2-1)\omega_2\ ,$$

introduced by the functions $\Sigma_1(z)$ and $\Sigma_2(z)$. Formulas (12a) and (12b) define the functions $\Sigma_1(z)$ and $\Sigma_2(z)$ on the first (physical) Riemann sheet. These functions can be analytically continued to the second Riemann sheet, which is reached from the first sheet when one crosses the branch cut on the positive real axis, while going to the lower half plane. Therefore the analytic functions $G_g(z)$, $G_1(E,z)$, and $G_2(E,z)$ are also defined on a multisheet complex surface. They may have also, in general, real and complex poles.

In order to obtain the time-dependent amplitudes $U_g(t)$, $U_1(E,t)$, and $U_2(E,t)$ one could close the con-

tour of integration, which appears in Eq. (9), by adding the half-circle in the lower half of the second Riemann sheet and a contour around the negative part of the real axis (up to the branch point) which would take one back to the starting point on the first Riemann sheet.

Here, I will concentrate only on the long time behavior of the atomic system, having in mind the ionization process induced by a cw laser or a pulse of long duration.

III. ENERGY DISTRIBUTION OF THE PHOTOELECTRONS

The behavior of the system at $t=\infty$ is determined by the residues of the analytic functions $G_g(z)$, $G_1(E,z)$, and $G_2(E,z)$ at the real poles. The remaining poles and other singularities contribute only to the transient effects. The function $G_g(z)$ has no real poles. It means that at the end the bound state will be completely depopulated; the atom will be completely ionized. Functions $G_1(E,z)$ and $G_2(E,z)$ have one real pole each, at

$$z_1=E+(n_1-1)\omega_1+n_2\omega_2$$

and at

$$z_2=E+(n_1-1)\omega_1+(n_2-1)\omega_2,$$

respectively. The probability densities to find the electron with the parity specified by the indices 1 and 2 are given by the expressions

$$W_1(E)=|U_1(E,t\to\infty)|^2, \tag{13a}$$

$$W_2(E)=|U_2(E,t\to\infty)|^2, \tag{13b}$$

or, in other words, the functions $W_1(E)$ and $W_2(E)$ describe the energy spectra of the final electrons.

Using my solution (10), I arrive at the following expressions for $W_1(E)$ and $W_2(E)$:

$$W_1(E)=n_1|D_1(E)|^2/|(E-E_g-\omega_1)\{1-\lambda^2 n_2[S_1(E)-i\gamma_1(E)][S_2(E+\omega_2)-i\gamma_2(E+\omega_2)]\}-n_1[S_1(E)-i\gamma_1(E)]|^2, \tag{14a}$$

$$W_2(E)=\lambda^2 n_1 n_2|D_2(E)|^2|S_1(E-\omega_2)-i\gamma_1(E-\omega_2)|^2/|(E-E_g-\omega_1-\omega_2)\{1-\lambda^2 n_2[S_1(E-\omega_2)-i\gamma_1(E-\omega_2)]\times[S_2(E)-i\gamma_2(E)]\}-n_1[S_1(E-\omega_2)-i\gamma_1(E-\omega_2)]|^2. \tag{14b}$$

The functions $S_1(E)$ and $\gamma_1(E)$ are the real and the imaginary parts of the analytic function $\Sigma_1(z)$ calculated at the point $z_1+i\epsilon$ $(\epsilon\to 0+)$,

$$S_1(E)=\mathbb{P}\int_{E_0}^{\infty}dE'\frac{|D_1(E')|^2}{E-E'},\qquad \gamma_1(E)=\pi|D_1(E)|^2, \tag{15a}$$

where the symbol $\mathbb{P}$ indicates the principal part of the integral. Similarly, $S_2(E)$ and $\gamma_2(E)$ are the real and the imaginary parts of the function $\Sigma_2(z)$ calculated at the pole $z_2+i\epsilon$ $(\epsilon\to 0+)$,

$$S_2(E)=\mathbb{P}\int_{E_0}^{\infty}dE'\frac{|D_2(E')|^2}{E-E'},\qquad \gamma_2(E)=\pi|D_2(E)|^2. \tag{15b}$$

To proceed further, we must specify the functions $|D_1(E)|^2$ and $|D_2(E)|^2$.

As a special case I will consider now two symmetric, Lorentzian profiles $|D_1(E)|^2$ and $|D_2(E)|^2$, both centered far from the ionization edge E_0. In accordance with the assumptions of the model, I assume that $|D_1(E)|^2$ is centered at the energy E_1 close to $E_g+\omega_1$, whereas $|D_2(E)|^2$ is centered at E_2 which lies close to $E_g+\omega_1+\omega_2$ (see Fig. 1).

$$|D_i(E)|^2=\frac{f_i^2}{(E-E_i)^2+A_i^2},\quad i=1,2. \tag{16}$$

If $E_i-E_0\gg A_i$ for both profiles, then it is a good approximation to shift the lower limit in the integral defining $S_i(E)$ from E_0 to $-\infty$ and to obtain[8]

$$S_i(E)-i\gamma_i(E)=\frac{g_i}{E-E_i+iA_i},\quad i=1,2. \tag{17}$$

The quantities g_1 and g_2,

$$g_i=\frac{\pi f_i^2}{A_i}=\int_{-\infty}^{\infty}dE\,|D_i(E)|^2,\quad i=1,2 \tag{18}$$

measure the strength of the effective coupling with the whole profiles.

Inserting those expressions for S_1, S_2, γ_1, and γ_2 into the general formulas for $W_1(E)$ and $W_2(E)$, we obtain

$$W_1(E)=\Omega_1^2 A_1[(E-E_2+\omega_2)^2+A_2^2]/\pi P(E), \tag{19a}$$

$$W_2(E)=\Omega_2^2\Omega_1^2 A_2/\pi P(E-\omega_2), \tag{19b}$$

where

$$P(E)=\{(E-E_g-\omega_1)[(E-E_1)(E-E_2+\omega_2)-A_1A_2-\Omega_2^2]-\Omega_1^2(E-E_2+\omega_2)\}^2$$
$$+\{(E-E_g-\omega_1)[(E-E_1)A_2+(E-E_2+\omega_2)A_1]-\Omega_1^2A_2\}^2 , \quad (20)$$

and I have defined

$$\Omega_1=(n_1g_1)^{1/2}, \quad \Omega_2=\lambda(n_2g_1g_2)^{1/2} . \quad (21)$$

The quantity Ω_1 can be interpreted as a generalized Rabi frequency of the first transition, as will be seen later. Similarly, Ω_2 plays the role of a generalized Rabi frequency of the second transition (within the continuum). Notice that the intensities n_1 and n_2 of two laser beams, as well as the quantities g_1 and g_2, enter only through Ω_1 and Ω_2.

Both energy distribution functions $W_1(E)$ and $W_2(E)$ were studied numerically for different values of widths A_1 and A_2 of the profiles $|D_1(E)|^2$ and $|D_2(E)|^2$, for different detunings Δ_1 and Δ_2,

$$\Delta_1=E_1-(E_g+\omega_1) , \quad (22a)$$

$$\Delta_2=E_2-(E_g+\omega_1+\omega_2) , \quad (22b)$$

and for different ratios of the two Rabi frequencies,

$$R=(\Omega_2/\Omega_1)^2 . \quad (23)$$

Since I use the units in which $\hbar=1=c$, all quantities have the dimensions of powers of energy (frequency). The quantity Ω_1 will serve as a universal unit of energy.

The spectrum of the photoelectrons consists of two parts: one centered around $E_g+\omega_1$ and described by $W_1(E)$ and the other centered around $E_g+\omega_1+\omega_2$ and described by $W_2(E)$. Both parts have an interesting structure due to the strong influence of the laser beams, which causes the effects analogous to the dressing of the atom in the bound-bound transitions. If the widths A_1 and A_2 of the profiles $|D_1(E)|^2$ and $|D_2(E)|^2$ are small, as compared to the Rabi frequencies, each part of the spectrum will be split into three peaks. The typical shapes of the spectra are shown in Fig. 2 at the exact resonance ($\Delta_1=0=\Delta_2$) and for equal Rabi frequencies ($R=1$). We see that the splitting is clearly visible for $A_1=0.25\Omega_1=A_2$ and disappears when $A_1=\Omega_1=A_2$. It is worth noticing that the splitting will appear also when only one profile is narrow (for example, the splitting was observed for $A_1=\Omega_1$, $A_2=0.2\Omega_1$ or for $A_1=0.1\Omega_1$, $A_2=2\Omega_1$).

The distance between the central peak and outer peaks [the same for $W_1(E)$ and for $W_2(E)$] for narrow profiles is equal to

$$[\Omega_1^2+\Omega_2^2+(\Delta_1/2)^2]^{1/2}$$

when Δ_2 vanishes. This shows that Ω_1 and Ω_2 indeed play the role of the generalized Rabi frequencies.[9]

Despite some similarities, the shapes of two functions $W_1(E)$ and $W_2(E)$ are quite different. In $W_2(E)$ the central peak always dominates, whereas in $W_1(E)$ outer peaks are often quite pronounced. For narrow profiles they will dominate.

This splitting of the spectrum is analogous to the ac Stark splitting known for bound-bound transitions. I believe that it is not due to the special form of my model. It is, probably, a characteristic feature of the cc transitions induced by very intense laser beams, when they are nearly resonant with some autoionizing states or other singularities of the density of states in the continuum. Unfortunately, this splitting would be very difficult to observe experimentally. It would probably be easier to observe the structure of the spectrum indirectly, in the experiment in which one collects photoelectrons above a

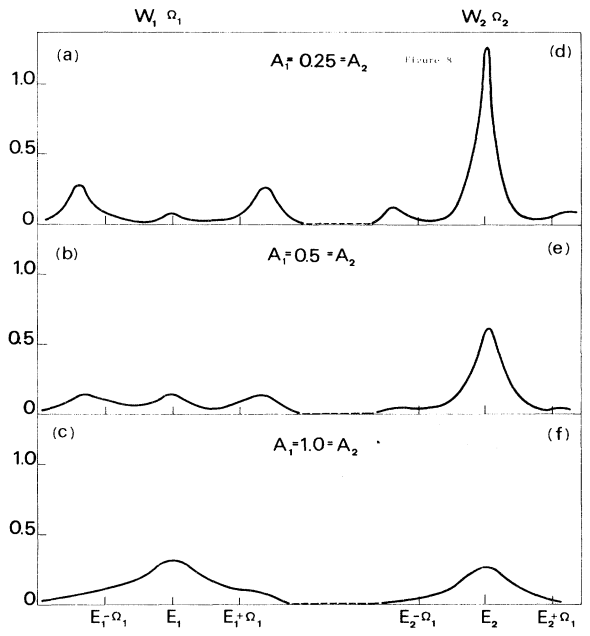

FIG. 2. Energy distribution of photoelectrons. The first part of the spectrum, described by $W_1(E)$ is shown in (a), (b), and (c). The second part, described by $W_2(E)$ is shown in (d), (e), and (f). This part is shifted from the position of the first part by the energy ω_2. All functions were calculated at the exact resonance ($\Delta_1=0=\Delta_2$) and for equal Rabi frequencies ($R=1$). Diagrams (a) and (d) correspond to $A_1=0.25\Omega_1=A_2$; diagrams (b) and (e) to $A_1=0.5\Omega_1=A_2$; diagrams (c) and (f) to $A_1=\Omega_1=A_2$.

certain threshold energy V_0. The measured number of photoelectrons from the first part of the spectrum with energies above the threshold determines the probability $\bar{P}_1$,

$$\bar{P}_1 = \int_{V_0}^{\infty} dE\, W_1(E) . \tag{24}$$

This is a function of the energy difference V,

$$V = E_g + \omega_1 - V_0 . \tag{25}$$

The function $\bar{P}_1$ was calculated from Eq. (19a) and is plotted in Fig. 3 for the same values of all the parameters that were used to obtain the spectrum shown in Fig. 2(a) (i.e., for $A_1 = 0.25\Omega_1 = A_2$, $\Delta_1 = 0 = \Delta_2$, $R = 1$). Notice that the negative values of V correspond to the threshold energy V_0 larger than the central energy E_1 of the profile $D_1(E)$ (E_1 coincides with $E_g + \omega_1$ at the exact resonance). We see that the probability $\bar{P}_1$ increases with increasing V. This is quite obvious, because with lower V_0 more electrons are being collected. What is worth noticing is the slope of the curve. There are two regions where $\bar{P}_1$ grows rapidly (near $V = -1.4\Omega_1$ and near $V = 1.4\Omega_1$). They coincide with the positions of the outer peaks in the spectrum $W_1(E)$. The evidence of the central peak in $\bar{P}_1$ is weak because of the smallness of the peak itself.

We will now study the integrals

$$P_1 = \int_{E_0}^{\infty} dE\, W_1(E) \tag{26a}$$

and

$$P_2 = \int_{E_0}^{\infty} dE\, W_2(E) . \tag{26b}$$

P_1 and P_2 are the probabilities that a photoelectron belongs to the first or the second part of the spectrum, respectively. Those two groups of electrons differ not only in their energies but also in parity; they are described by different partial waves. Of course, P_1 and P_2 must satisfy the relation

$$P_1 + P_2 = 1 ,$$

because at $t = \infty$ the atom is completely ionized.

The probability P_2 is plotted in Fig. 4 as a function of R (i.e., a function of the intensity n_2 of the second laser beam when the intensity n_1 of the first beam is kept fixed). Both curves in Fig. 4 correspond to the exact resonance; they are calculated for different values of the widths A_1 and A_2. We see that P_2 is a nonlinear function of R and that the nonlinearity is stronger for smaller values of A_1 and A_2. However, the ratio P_2/P_1 is almost linear in R for values of R from $Q2$ up to 2.5 (see Fig. 5). This property was checked for different values of A_1 and A_2 (not necessarily equal) at the exact resonance.

The probabilities P_1 and P_2 also depend strongly on the widths A_1 and A_2 of two profiles $D_1(E)$ and $D_2(E)$. This dependence was checked at the exact resonance. The results for equal Rabi frequencies ($R = 1$) are given in Table I. We see that for narrow profiles the probability P_2 is greater than P_1; the second part of the spectrum contains more electrons than the first. For wider profiles (of the order Ω_1) the situation is reversed; $P_1 > P_2$, and there are more electrons in the first part of the spectrum. This property is also evident in Fig. 5, where the ratio P_2/P_1 is plotted as a function of R for different values of A_1 and A_2. We see that the line (d) for $A_1 = \Omega_1 = A_2$ lies below all remaining lines that correspond to the smaller values of A_1 and A_2.

The effects of detunings on the numbers of the

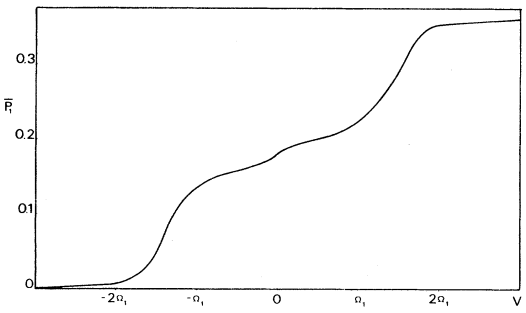

FIG. 3. Probability $\bar{P}_1$ [defined by Eq. (24)] vs the distance V between the resonant energy $E_g + \omega_1$ and the threshold energy V_0. This probability was calculated at the exact resonance ($\Delta_1 = 0 = \Delta_2$) for equal Rabi frequencies ($R = 1$) and for $A_1 = 0.25\Omega_1 = A_2$.

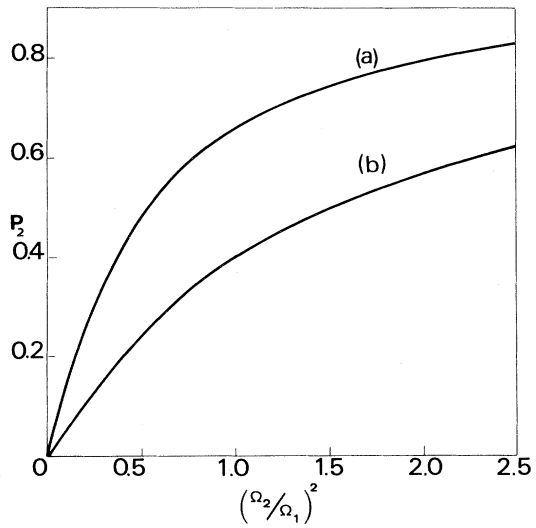

FIG. 4. Probability P_2 [defined by Eq. (26a)] vs the ratio of the Rabi frequencies squared $(\Omega_2/\Omega_1)^2$ calculated at the exact resonance. Function P_2 in (a) was calculated for narrow profiles, $A_1 = 0.1\Omega_1 = A_2$. Diagram (b) corresponds to broad profiles, $A_1 = \Omega_1 = A_2$.

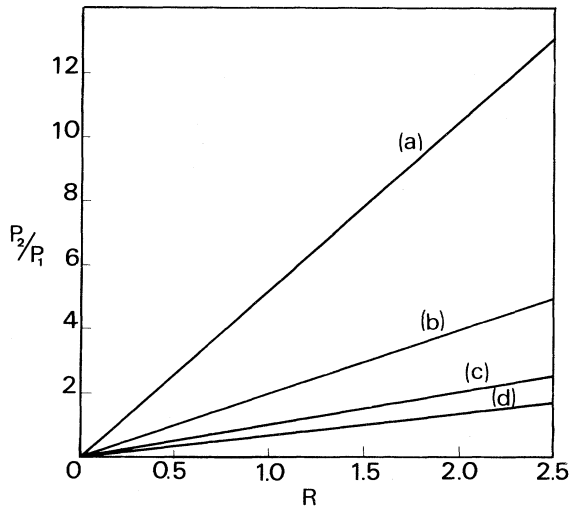

FIG. 5. Ratio of probabilities P_2/P_1 vs R, $R=(\Omega_2/\Omega_1)^2$, calculated at the exact resonance for (a) $A_1=0.1\Omega_1$, $A_2=\Omega_1$, (b) $A_1=0.1\Omega_1=A_2$, (c) $A_1=\Omega_1$, $A_2=0.1\Omega_1$, and (d) $A_1=\Omega_1=A_2$.

photoelectrons in the first and the second part of the energy spectrum was also studied. In Fig. 6 the probability P_2 is plotted for equal Rabi frequencies ($R=1$) and narrow profiles ($A_1=0.25\Omega_1=A_2$) in three different situations. The curve (a) corresponds to the situation when the frequency ω_2 of the second laser beam is fixed at the resonant value and the frequency ω_1 of the first beam is swept across its resonant value. Both detunings Δ_1 and Δ_2 are equal in this case, since Δ_2 denotes the total detuning. The curve (b) corresponds to the situation when the frequency ω_1 is fixed at the resonance ($\Delta_1=0$) while ω_2 varies around its resonant value (Δ_2 varies around zero). We see that this curve differs little from the curve (a). It indicates that a partial detuning in the first transition affects P_2 only slightly if there is a total detuning. In both cases the probability P_2 decreases with increasing total detuning. The curve (c) corresponds to the situation when the frequency ω_1 is swept across the resonant value, but there is no total detuning ($\Delta_2=0$). In this case the probability P_2 attains its minimum at the resonance. It is worth noticing that all peaks are very broad, their widths being much larger (about eight times) than the widths of the profiles which, in this case, are both equal to $0.25\Omega_1$.

TABLE I. The values of the probabilities P_1 and P_2 calculated at the exact resonance and for equal Rabi frequencies for different values of the widths A_1 and A_2. A_1 and A_2 are measured in units of Ω_1.

A_1	A_2	P_1	P_2
0.1	0.1	0.34	0.66
0.25	0.25	0.36	0.64
0.5	0.5	0.43	0.57
1.0	1.0	0.60	0.40
1.0	0.1	0.50	0.50

All effects discussed above occur when both profiles $D_1(E)$ and $D_2(E)$ are located so far from the edge of the continuum that the position of the edge has a negligible influence on the dynamics of the process. I shall now study the effect of the edge of the continuum on the energies of the photoelectrons when one profile $D_1(E)$ is centered close to the edge. The second profile $D_2(E)$ is centered at a much higher energy in the continuum; the functions $S_2(E)$ and $\gamma_2(E)$ will be assumed in the previous form [see Eq. (17)].

The function $|D_1(E)|^2$ will be assumed in the form

$$|D_1(E)|^2=\frac{f_1^2(E-E_0)^{1/2}}{[(E-E_1)^2+A_1^2][(E_1-E_0)^2+A_1^2]^{1/4}}\ . \tag{27}$$

The function $(E-E_0)^{1/2}$ is chosen in accordance with the general results obtained by Wigner[10] in his study of the threshold effects. The factor $[(E_1-E_0)^2-A_1^2]^{1/4}$ was introduced in order to guarantee that, in the limit of a very large distance between the edge E_0 and the center E_1 of the profile, the function $|D_1(E)|^2$ collapses to its previous form.

Inserting Eq. (27) into Eq. (15a), which defines the functions $S_1(E)$ and $\gamma_1(E)$, we obtain

$$\gamma_1(E)=\frac{\pi f_1^2}{(E-E_1)^2+A_1^2}\frac{(E-E_0)^{1/2}}{[(E_1-E_0)^2+A_1^2]^{1/4}}\ , \tag{28a}$$

$$S_1(E)=\frac{\pi f_1^2}{(E-E_1)^2+A_1^2}\frac{1}{2[(E_1-E_0)^2+A_1^2]^{1/2}}\left[\frac{E-E_1}{\sin\phi}-\frac{A_1}{\cos\phi}\right], \tag{28b}$$

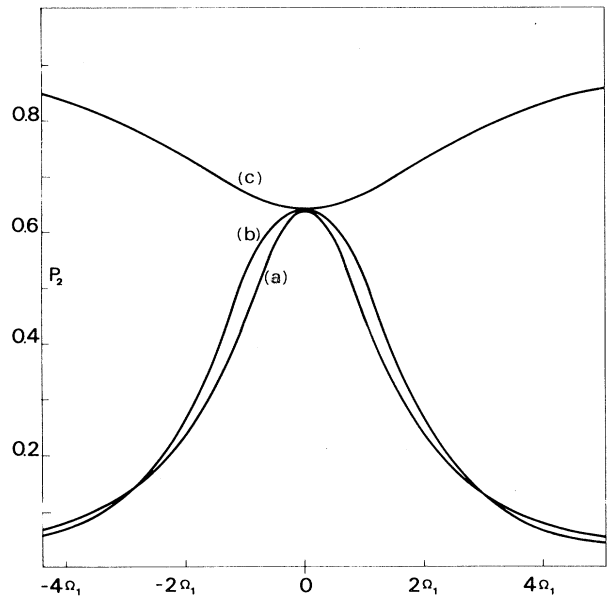

FIG. 6. Effect of detunings on the probability P_2. (a) P_2 vs Δ_2 for $\Delta_1=\Delta_2$; (b) P_2 vs Δ_2 for $\Delta_1=0$; (c) P_2 vs Δ_1 for $\Delta_2=0$. All three curves were calculated for equal Rabi frequencies and for $A_1=0.25\Omega_1=A_2$.

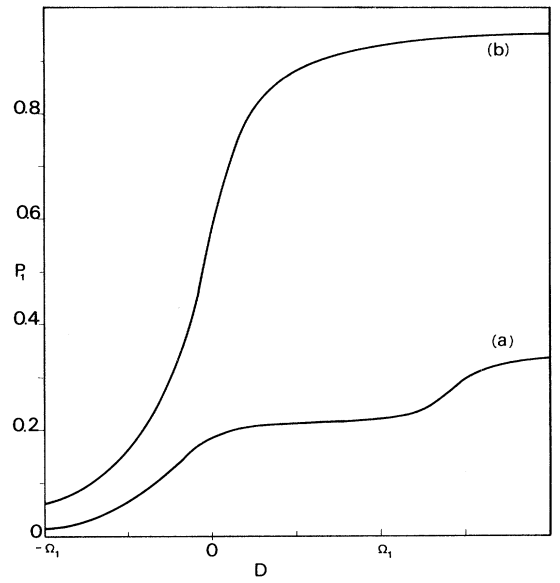

FIG. 7. Effect of the edge on the probability P_1. (a) P_1 vs the distance D between the edge E_0 of the continuum and the resonant energy $E_g+\omega_1$, calculated at the exact resonance for equal Rabi frequencies. (b) Integral $\int_{E_0}^{\infty} dE\,|D_1(E)|^2$ in arbitrary units vs the distance D of the edge.

where

$$\phi=\tfrac{1}{2}\arctan[A_1/(E_1-E_0)]\ . \tag{29}$$

In what follows, the distance between $E_g+\omega_1$ and the edge E_0 (see Fig. 1) is denoted by D,

$$D=E_g+\omega_1-E_0\ .$$

The curve (a) in Fig. 7 shows the dependence of the probability P_1 (which determines the number of the photoelectrons in the first part of the spectrum) on the distance D. It was calculated at the exact resonance ($\Delta_1=0=\Delta_2$) for equal Rabi frequencies ($R=1$) and for the widths $A_1=0.25\Omega_1=A_2$. Again, we see the evidence of a strong influence of the laser light on the energy structure of the atom. There is a pronounced change in P_1 for D around the value of 1.4 Ω_1 although in this case the edge E_0 of the continuum is separated from the center of the profile $D_1(E)$ by a distance which is six times larger than the width of the profile. The curve (b) in Fig. 7 shows the integral

$$\int_{E_0}^{\infty} dE\,|D_1(E)|^2$$

in arbitrary units as a function of D. We see that in the region around $D=1.4\Omega_1$ this integral varies very little. Its decrease cannot be responsible for a rapid decrease of P_1.

IV. CONCLUDING REMARKS

The properties of the energy distribution of the photoelectrons, studied in this paper, indicate that a strong laser field not only induces optical transitions in the continuum, but also modifies its structure. The appearance of several distinct maxima in the energy distribution is an analog of the ac Stark splitting of the discrete energy levels. The light broadening was observed in all lines in Fig. 7 obtained when one or both frequencies of laser beams were being swept across the resonance. Thus the atomic system which consists of one bound state and the continuum with two regions of high density of states resembles a three-level atom. However, the presence of the continuum introduces one essentially new feature. Strong laser beams may depopulate completely the initial bound state. The dressing of the atom in the laser field manifests itself also in various edge effects, which can, of course, be studied only in the presence of the continuum.

ACKNOWLEDGMENTS

I would like to thank the Departments of Physics of the University of Southern California and the

University of Rochester for their hospitality during the time when part of this work was completed. I am also very grateful to Professor I. Bialynicki-Birula, Professor P. Lambropoulos, and Professor J. H. Eberly for many illuminating and helpful discussions and suggestions. This work was partially supported by the U.S. Air Force Office of Scientific Research at the University of Rochester.

[1]P. Agostini, F. Fabre, G. Mainfray, G. Petite, and N. K. Rahman, Phys. Rev. Lett. 42, 1127 (1979); F. Fabre, G. Petite, P. Agostini, and M. Clement, J. Phys. B 15, 1353 (1982).

[2]This terminology was explained in detail by P. Lambropoulos, Appl. Opt. 19, 3926 (1980).

[3]Recently, S. Klarsfeld and A. Maquet calculated the probability of the cc transition in hydrogen within the framework of the perturbation theory, using Padé-Sturmian approximation [J. Phys. B 12, L553 (1979); Phys. Lett. 78A, 40 (1980)].

[4]This phenomenon was explained theoretically by U. Fano, Phys. Rev. 124, 1866 (1961).

[5]K. Rzążewski and J. H. Eberly, Phys. Rev. Lett. 47, 408 (1981).

[6]P. Lambropoulos and P. Zoller, Phys. Rev. A 24, 379 (1981).

[7]B. L. Beers and L. Armstrong, Phys. Rev. A 12, 2447 (1975).

[8]In this case the branch points z_1 and z_2 are moved to infinity and different Riemann sheets are not connected to each other. Therefore the contribution to the amplitudes $U_i(t)$ due to the existence of branch points vanishes.

[9]The second reason to call Ω_1 and Ω_2 the generalized Rabi frequencies is related to the transient effects which are not discussed here. For narrow profiles, Ω_1 and Ω_2 determine the frequencies of the oscillations of the amplitudes $U_g(t)$, $U_1(E,t)$, and $U_2(E,t)$.

[10]E. P. Wigner, Phys. Rev. 73, 1002 (1948).